Study on efficient adsorption of mb by chitosan-polyvinyl alcohol composite hydrogels doped with nano-SiO_2 and GO

B. Yuan [a], F. Liang [a], C. Li [a,b,*], Y. Jiang [b], J. Sun [b], Y. Tao [c], A. Amirfazli [d]

[a] *School of Materials Engineering, Jiangsu University of Technology, Changzhou, 213001, P. R. China*

[b] *School of Mechanical Engineering, Nantong Institute of Technology, Nantong,226002, P. R. China*

[c] *School of Art and Design, Changzhou Institute of Technology, Changzhou,213032, P. R. China*

[d] *Department of Mechanical Engineering, York University, Toronto, ON, M3J 1P3, Canada*

This study used a straightforward one-pot method was accustomed to prepare a composite hydrogel prepared with polyvinyl alcohol (PVA) and chitosan (CS) as substrates doped with hydrophilic nano-sio2 and GO. The composition and structure of the composite hydrogel were characterized by SEM, XRD, XPS, etc, as well the tensile and compression tests were carried out. The effects of temperature, pH, concentration of adsorbent and other related parameters on adsorption properties were studied. Adsorption kinetics and the adsorption process was fitted using adsorption isotherm models of composite hydrogels. The results show that the hydrogel both has excellent mechanical characteristics, and has strong adsorption properties for methylene blue (MB) in dye wastewater. The maximum tensile strength of the composite hydrogel exceeds 1750kPa, the maximum tensile displacement is 300% of the initial form, and the maximum compressive strength exceeds 13000kPa. This is mainly due to the enhancement of nano-sio2 and the hydrogen bond interaction between the molecules. The optimum adsorption temperature of methylene blue was 55℃, pH was 7.0, and the concentration of adsorbent was 5%. PCG three-dimensional network structure composite hydrogel might be utilised as an inexpensive, sustainable and effective adsorbent for the removal of dye industry wastewater in textile industry, and has broad industrial application prospects.

(Received May 9, 2025; Accepted August 8, 2025)

Keywords: Hydrogel, Polyvinyl alcohol, Nano-silica, High mechanical properties, Adsorb

1. Introduction

With the advancement of the global process of industrialization, the utilization of heavy metals and dyes has increased significantly [1]. While enriching human life, these substances also

* Corresponding author: cql6660607@163.com

https://doi.org/10.15251/DJNB.2025.203.931

lead to important consequences in terms of water pollution. Industrial effluent penetrates into people body through complex water network, causing great harm to life and health of human [2-4]. Conventional techniques like ion exchange, chemical precipitation, photocatalysis, and biological techniques have been used for wastewater purification to get rid of dyes and heavy metal cations[5]. But real-world implementation of these techniques faces challenges due to high costs, complex processing procedures, and the potential for secondary pollution during recycling [6-7].

The adsorption and ion exchange mechanisms are employed in the adsorption mechanism. So as to facilitate sewage treatment, the adsorption material generates a variety of intermolecular interactions between the surface group and the target ions of heavy metals when the adsorption process [8]. These forces include intermolecular forces such as ionic bonds, hydrogen bonds and coordination bonds. In the case of dye molecules, They cling to substantial things surfaces by physical interactions (hydrogen bonding, van der waals force), chemical interactions as well as ion exchanges in adsorption, and can be successfully extracted from sewage [9-10]. The examination of wastewater treatment techniques for contamination by heavy metals and dyes shows the enormous research opportunity of adsorbent techniques. Activated carbon, Common adsorbents include hydrogel and inorganic silica gel [11]. However, activated carbon adsorbents are hampered by being expensive and conventional, which limits their large-scale application. In the instance of silica gel, they generally have weak thermal stability and a low adsorption capability. The adsorption rate of microporous silica gel decreases experiences difficulties with desorption in low humidity situations, while the desorption rate of macroporous silica gel exhibits greater porosity, but the capacity for adsorption is restricted [12-15]. The unique three-dimensional network structure of hydrogel adsorbents, comprising several hydrophilic groups (-OH, -COOH). These groups can retain substantial quantities of water and interact with heavy metal ions. Therefore, hydrogel adsorbents show significant adsorption capacity for heavy metal ions, which has attracted the attention and interest of researchers for use and future development [16]. Hydrogels are the most often utilized adsorbent materials; they can be classified as either natural or manufactured. The synthetic hydrogel has excellent mechanical properties, high expansion rate and long service life [17]. Nevertheless, the majority of artificial hydrogel materials are derived from petrochemical products, which lack of biodegradability and renewability, resulting in environmental pollution problems. Therefore, investigating materials made of natural polymers has been paid more and more attention. Natural polymer hydrogels can absorb nutrient-rich materials, heavy metals, other water-based contaminants and dyes thanks to their chemical groups, and thus have further potential for wastewater treatment [18-20]. Natural polymer hydrogels have the advantages of abundant resources, high cost performance, good biocompatibility and biodegradability [21]. Due to the abundant amino, natural polymer hydrogels have outstanding adsorption qualities, hydroxyl groups and carboxyl that can interact with dyes and heavy metal ions. Therefore, research on hydrogel adsorbents made of natural polymers is very important [22]. A type of economical alkaline polysaccharide found in nature, chitosan (CS) has remarkable adsorption characteristics and the potential to be utilised extensively in wastewater treatment. A large number of chitosan's free active groups possess the capability to bind transition metal cations to promote the process of agglomeration and adsorption, in order to attain the objective of wastewater treatment [23]. Chitosan exhibits exceptional biocompatibility, decomposability, as well as other qualities [49]. Using a straightforward two-step process, Wu et al. created a sulfonic acid modified chitosan/poly N-isopropylacrylamide complex hydrogel and demonstrated it ability to adsorb heavy metal ions like Cu and Pb from sewage, wit 172 mg/g and

69 mg/g, respectively, are the highest adsorption capacities [24-26]. DNA-CS hydrogels were created by Chan et al. via in-situ DNA polymerization with opposite charge and chitosan polyelectrolyte through electrostatic crosslinking. Because there are a lot of cations and anions in the hydrogel, it has remarkable impact of desorption on heavy metal ions, cationic dyes, and anionic dyes [27-28]. Cellulose is often utilized in the treatment of wounds and drug-controlled release. Cellulose hydrogels are non-toxic, biodegradable and have excellent biocompatibility. They are excellent environmentally friendly biomaterials [29]. In addition, cellulose hydrogels have great potential in wastewater treatment. Wang prepared high crosslinking polyvinyl alcohol / carboxymethyl cellulose hydrogel, for Ni, Cu, Zn and other heavy metal ions have good adsorption performance, under alkaline conditions by chemical crosslinking cellulose-carboxymethyl cellulose/clay hydrogel, has good adsorption effect of methylene blue, the maximum removal rate of 98% [30]. One interesting approach is to form nanoscale silica in situ in biopolymers, rather than directly incorporating silica nanoparticles into the polymer matrix [31]. Hybridization of biopolymers with nanoscale silica has been applied in several fields. In addition, As they can protonate in acidic environments and deprotonate in neutral ones, bio-derived composite hydrogels containing nitrogen (N) and oxygen (O) functional groups have a high adsorption capacity [32-35]. This allows them to use ion exchange, hydrogen bonding, and electrostatic attraction to adsorb pollutants that are negatively and positively charged. In this study, chitosan and silica nanoparticles were incorporated into the PVA skeleton in a harmonious ratio and were compatible with each other, aiming to develop anion-trapping nanocomposite hydrogels with amino functional groups and rich carboxyl [36]. Using chitosan (CS) and polyvinyl alcohol (PVA) as matrix substances, PCG composite hydrogels were prepared by doping hydrophilic silica and graphene oxide in the matrix to improve the adsorption capacity of natural polymer hydrogels and mechanical properties. Various characterization methods were used to evaluate its synthetic state, test its swelling and mechanical properties, and use it as a natural adsorbent for adsorption of MB. Using PVA and CS as the skeleton of hydrogel, on the one hand, the insufficient adsorption capacity of PVA hydrogel is solved, and the influence of traditional CS hydrogel skeleton is also solved [37]. Further doping of nano-silica and graphene oxide can improve the silica mechanical properties of high-molecular weight polymer networks, and enhance the adsorption capacity of MB by using functional groups containing oxygen on graphene oxide's surface [38].

2. Experimental part

2.1. Materials

Polyvinyl alcohol (PVA, solubility /mol≥98, viscosity :45.0-55.0/mPa•s, average degree of polymerization is 1750 ± 50,) and methylene blue (MB) were purchased from Sinopharm Chemical Reagent Co., LTD. Chitosan (CS, molecular weight of unit 161.2) was purchased from Tianjin Zhonglian Chemical Co., LTD. Graphene oxide (GO, thickness: 5nm, layer diameter: 0.4-10μm) purchased from Jisheng Carbon Fiber (Guangdong) Co., LTD. Hydrophilic nano silica (20nm), hydrochloric acid (HCl) and sodium hydroxide (NaOH) are all supplied by Shanghai McLean Biochemical Technology Co., LTD. All commercially available reagents purchased are analytical grade and can be used without further purification.

2.2. Preparation of composite hydrogel

Firstly, 1.0g of chitosan was weighed and fully dissolved in 45ml of 2% acetic acid solution, then 0.25g of graphene oxide was added and the beaker was placed in an ultrasonic shaker for 30 minutes to ensure uniform dispersion of graphene oxide. Then 5g of polyvinyl alcohol was weighed and poured into the beaker, and the beaker was agitated in a pulp while submerged in a water bath at 95°C for two hours. Secondly, after the polyvinyl alcohol is completely dissolved, the water bath's temperature is adjusted to 70°C, and 0.3g nano-silica is weighed into the beaker and stirred at low speed until completely dissolved. Finally, the prepared composite hydrogel was poured into the polytetrafluoroethylene mold and put into the freeze dryer, and the sample was taken out every six hours and thawed at 5°C for two hours, which was a freeze-thaw cycle, requiring five cycles of freeze-thaw. The prepared hydrogels were named as PCG 3D network composite hydrogels.

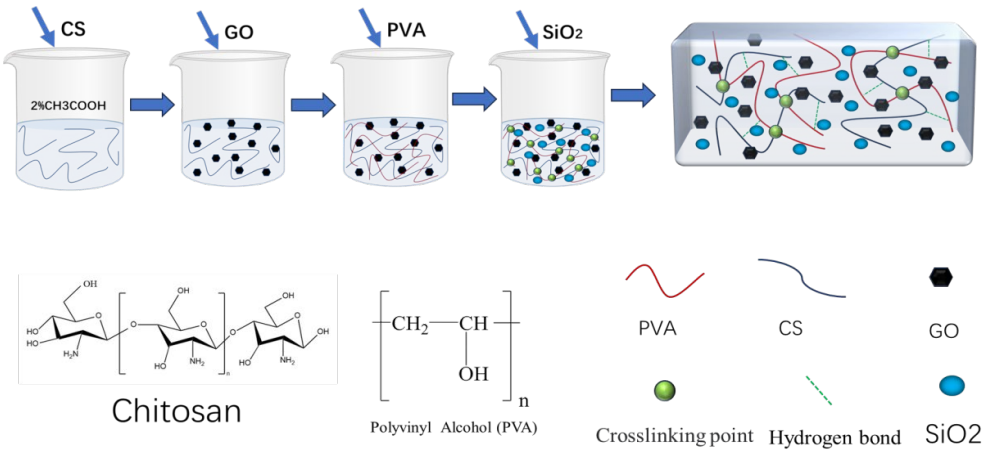

Fig. 1. PCG-SiO_2 Schematic diagram of gel preparation process.

2.3. Characterization of composite hydrogel

The fracture cross section of PCG-SiO2 hydrogel was observed by scanning electron microscope at the accelerated Voltage of 15 kilovolts. Before observation, the composite hydrogel specimens were freeze-dried and spattered with gold. The three-dimensional network hydrogels of PVA, CS, GO and PCG-SiO2 were characterized by Fourier transform infrared spectroscopy in the transmission mode of 4000-500 cm-1. Before observation, the dry hydrogels were first crushed with a grinder to obtain sample particles, and then the sample particles were ground into powder with a mortar [39]. Finally, the powder samples were mixed with KBr. Elemental analysis and quantitative spectrum of PCG-SiO2 3D network hydrogel before and after adsorption of methylene blue were carried out by X-ray photoelectron spectroscopy, and finally Gaussian function fitting was used. The thermal properties of the sample are analyzed using a thermogravimetric differential thermogravimetric (TG-DTG) analyzer, which heats the sample to ranging from 30°C to 600°C in increments of 10°C per minute in a nitrogen environment [40].

2.4. Water content and swelling test of hydrogel

2.4.1. Water retention test

The prepared PCG hydrogels and PCG-sio2 hydrogels were respectively weighed at their initial weights, and the two samples were weighed again every five hours at 25℃ until the weight of the two samples remained unchanged after complete dehydration. According to the starting weight as well as the ending weight, the water content of the two examples can be determined respectively, and the equation for calculating the water content is:

$$\text{Water content} = \frac{M_1 - M_2}{M_1} \times 100\% \quad (1)$$

M1: sample mass before dehydration, (g); M2: Mass of sample after complete dehydration, (g).

2.4.2. Swelling test

In order to study the qualities of swelling of the sample hydrogels, the PCG-sio2 hydrogels and lyophilised PCG hydrogels were placed in an oven at 60℃ until the weight of the hydrogels was completely dehydrated and remained unchanged, and their weights were weighed. Then the dried hydrogel sample was soaked in a phosphate solution with pH = 7.2 at 25 ° C, the sample was removed every five hours, the water on its surface was wiped and its weight was measured. Swelling equilibrium is reached until its weight is unchanged. The swelling ratio is calculated as follows:

$$\text{swelling ratio} = \frac{M_3 - M_4}{M_3} \times 100\% \quad (2)$$

M3: Mass after complete dehydration, (g);

M4: Mass after the sample reaches the swelling ratio, (g).

2.5. Mechanical properties of hydrogel

2.5.1. Tensile test

The mechanical tensile characteristics of composite hydrogels were studied using an universal tester that has a 100N sensor. The tensile rate of the machine under the condition of the machine is 50mm·min-1. All experimental samples were prepared in a customized teflon mold in dumbbell shape (length 50 mm, width 1mm, thickness 2 mm, sample after processing measured by a digital vernier caliper). At least 3-5 samples of each hydrogel were tested to obtain the average tensile strength, elongation at break and tensile modulus. Tensile fracture strain (ε) is delineated as:

$$\varepsilon = \frac{l - l_0}{l_0} \times 100\% \quad (3)$$

l: Stretch length of sample (mm);

l_0: Initial length of the sample (mm)

The formula for calculating tensile stress (σ) is:

$$\sigma = \frac{F}{A_0} \quad (4)$$

F: load force (N); A_0: Original cross-sectional area of sample (m2)

2.5.2. Compression test

The mechanical compression properties of composite hydrogel were studied by electronic universal testing machine. The mechanical compression rate was 3mm·min-1 under the condition of 250 N load cell. The cylindrical experimental sample (diameter 15mm, height 18mm, measured by digital vernier caliper after processing) was prepared by 24-well culture plate. At least 3-5 samples were tested for each group of hydrogels, and data such as average compression strength and compression modulus were obtained.

2.6. Adsorption performance test of hydrogel

2.6.1. Influence of different temperatures on adsorption performance

Methylene blue solution containing 150mg/L was prepared by simulating dye wastewater. First, prepare 4 beakers and pour 100ml of prepared solution into each beaker; Then the prepared circular thin slice sample hydrogel was divided into 4 pieces of uniform size and weighed to control the quality error of the sample, put into the beaker solution and covered with cling film; Then the six beakers were placed at 20℃, 35℃, 50 ° C and 65℃, and 5mL of the upper clear solution was taken out and placed in test tubes every 6 hours. Finally, UV-visible spectrophotometer (Agilent Cary 60 Agilent Technology Co., LTD., Malaysia) was used to detect the absorbance of the supernatant at 665nm, and the quantity of dye in the solution was computed using the solution's absorbance. The adsorption amount was calculated as follows:

$$Q_t = \frac{C_0 - C_t}{M} \times V \tag{5}$$

Q_t: the amount of dye adsorbed per unit mass of adsorbent (mg/g);
C_0: the initial concentration of dye (mg/L);
C_t: the dye concentration after adsorption at any time (mg/L);
M: the mass of adsorbent per liter of aqueous solution (g/L);
V: the volume of solution (L).

2.6.2. Effect of different pH on adsorption performance

First, prepare 4 beakers, pour 100ml of prepared solution into the beakers, and adjust the pH value to 4, 6, 7 and 8 respectively. Then divide the prepared circular sheet sample hydrogel into 4 pieces of uniform size and weigh them to control the sample quality error. Put them into the beaker solution and cover them with plastic wrap. Every 6 hours, 5mL of the upper clear solution was taken out and placed in a test tube. Finally, the absorbance of the supernuant was detected at 665nm by UV-VIS spectrophotometer, and in accordance with the resolution's absorbance, the dye concentration was computed.

2.6.3. Effect of different contents of GO on adsorption performance

Control the added GO content as (0.15g, 0.2g, 0.25g, 0.3g, 0.35g), prepare 5 beakers, pour 100ml of prepared solution into the beakers respectively, then divide the prepared circular thin slice sample hydrogel into 5 pieces of uniform size and weigh them to control the sample quality error, put them into the beaker solution and cover with plastic wrap. The beaker was placed at room temperature, and 5mL of the upper clear solution was taken out and placed in a test tube every 6

hours. Finally, the absorbance of the superserum was detected at 665nm used via UV-VIS spectrophotometry, and the concentration of dye in the solution was discovered by calculating the absorption of the mixture

2.6.4. Effect of different contents of CS on adsorption performance

Control the added CS content as (0.8g, 0.9g, 1.0g, 1.1g, 1.2g), prepare 5 beakers, pour 100ml prepared solution into the beakers respectively, then divide the prepared circular thin slice sample hydrogel into 5 pieces of uniform size and weigh them to control the sample quality error, put them into the beaker solution and cover with plastic wrap. The beaker was placed at room temperature, and 5mL of the upper clear solution was taken out and placed in a test tube every 6 hours. Finally, the absorbance of the superserum was detected at 665nm used via UV-VIS spectrophotometry, and the concentration of the dye in the solution was computed based on the absorbance of the solution.

2.6.5. Effect of different initial dye concentration on adsorption performance

Add 5ml, 10ml, 15ml and 20ml solution with a concentration of 150 mg/L into 4 beakers respectively, and then add deionized water until the volume of the solution in the beaker is 100ml. Then divide the prepared circular thin slice sample hydrogel into 4 pieces of uniform size and weigh them to control the sample quality error, put them into the beaker solution and cover them with plastic wrap. The beaker was placed at room temperature, and 5mL of the upper clear solution was taken out and placed in a test tube every 6 hours. Finally, the absorbance of the superserum was detected at 665nm used via UV-VIS spectrophotometry, and the dye concentration in the solution was computed based on the absorbance of the solution.

2.7. Adsorption kinetics

The experimental data of PCG-SiO_2 hydrogel adsorption of methylene blue solution were fitted by the experimental mechanism was examined utilising quasi-second-order adsorption kinetics and quasi-first-order.

The proposed primary order adsorption dynamical formula is expressed as follows:

$$\ln(q_e - q_t) = \ln q_e - k_1 t \tag{6}$$

q_e: adsorption capacity of adsorbent in equilibrium state (mg/g);
q_t: adsorption amount of adsorbent at different times (mg/g);
K_1: adsorption rate constant of pseudo-first order kinetic equation (min-1).
The proposed secondary adsorption kinetics equation is expressed as follows:

$$\frac{t}{q_t} = \frac{1}{k_2 {q_e}^2} + \frac{t}{q_e} \tag{7}$$

q_e: saturated adsorption capacity (mg/g);
q_t: adsorption capacity at different times (mg/g);
K_2: adsorption rate constant of pseudo-second order kinetics (g·mg/g·min)

2.8. Isothermal adsorption line

The experimental data of PCG-SiO2 hydrogel adsorption of methylene blue solution under different conditions were fitted utilizing Freundlich isothermal and Langmuir models to examine the experimental mechanism.

The equation of the isothermal line model of Langmuir adsorption is as follows:

$$\frac{C_e}{q_e} = \frac{1}{q_m} C_e + \frac{1}{q_m K_L} \tag{8}$$

C_e: concentration of adsorbate in solution at equilibrium (mg·L-1);
q_e: adsorption capacity of adsorbent at equilibrium (mg·g-1);
q_m: amount of adsorbate adsorbed by the adsorbate (mg·g-1);
K_L: Langmuir adsorption constant.

The equation of the isothermal line model of Freundlich adsorption is as follows:

$$\ln q_e = \frac{1}{n} \ln C_e + \ln K_f \tag{9}$$

q_e: adsorption capacity of adsorbent in equilibrium state (mg/g);
C_e: concentration of adsorbate in solution at equilibrium (mg/L);
K_f: Freundlich adsorption constant.

3. Results and analysis

3.1. Characterization analysis of hydrogel

3.1.1. SEM analysis

The SEM images of (a)-(f) at different magnifications in Figure 2 all show obvious pore and porous structures. The porosity of the hydrogel is important for the adsorption of dyes because it provides more surface area, which expands the region in contact with the molecule of methylene blue. The pore walls are mostly smooth, but slightly irregular morphology can be seen in some areas, which may be attributed to the addition of graphene oxide and nano-silica. The addition of nanomaterials usually results in the creation of a rough texture on the surface of the pore wall, thereby increasing the effective surface area of the pore and further improving the adsorption performance. The addition of nano-graphene oxide helps to increase the hydrogel's mechanical strength and provides more functionalized sites for adsorbing dye molecules [41]. Chitosan has good biocompatibility and amino functional group, which can also interact with methylene blue molecules to enhance the chemisorption effect. The pore wall of the hydrogel is thick and uniform, suggesting that it has good mechanical strength and structural stability. This is very advantageous for the practical application of composite hydrogels, because when adsorbing dyes, the material needs to maintain a certain stability in the aqueous phase without breaking. Due to the highly developed pore structure and the synergistic effect of different functional components, the composite hydrogel is anticipated to possess a high capacity for adsorption, especially under the dual action of large-scale physical adsorption and chemical bonding.

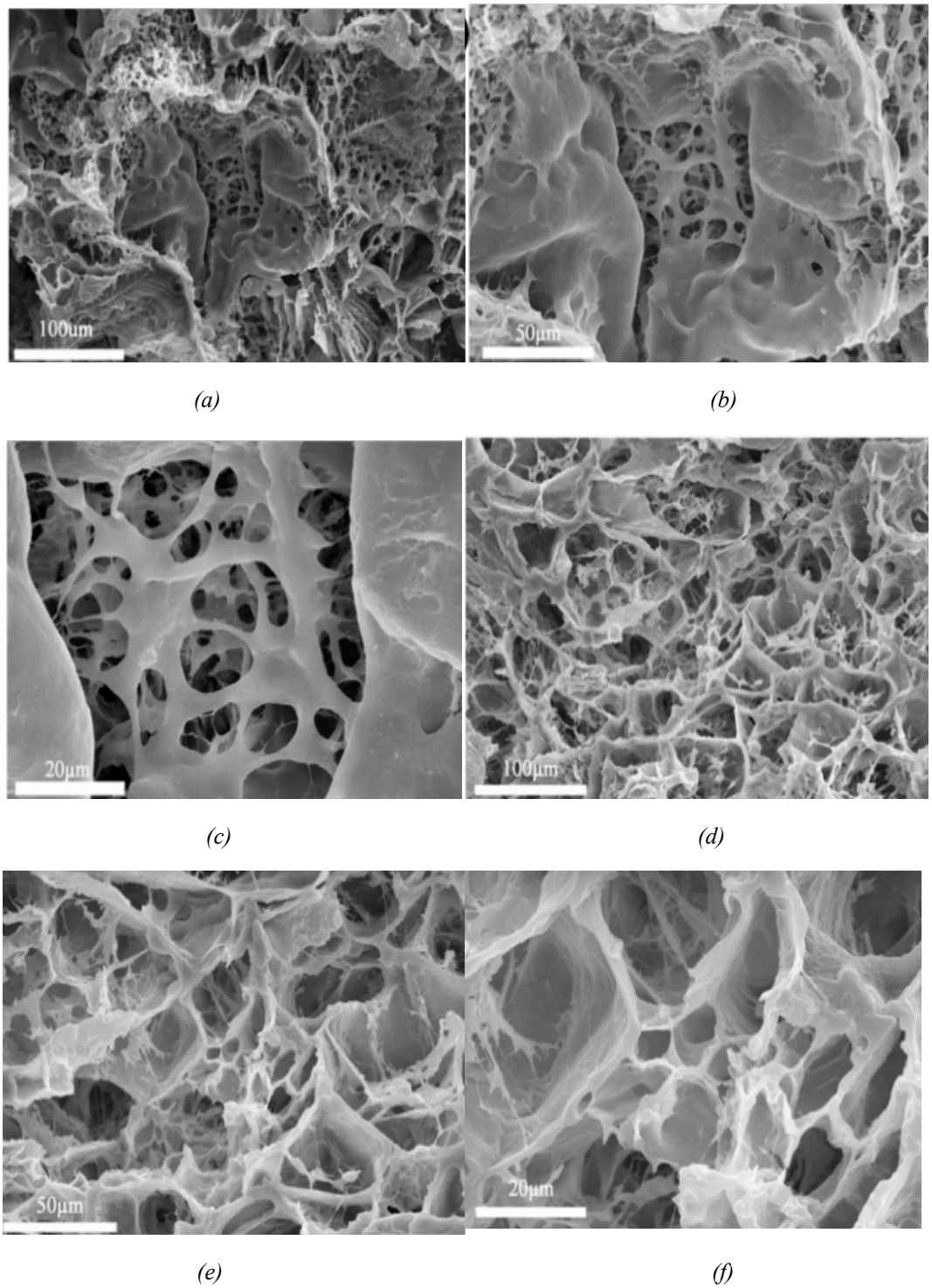

Fig. 2. PCG-SiO_2 SEM images of hydrogels at different magnifications.

3.1.2. FTIR analysis

Figure 3(a) show that the characteristic attains maximum 3233 cm^{-1} being equivalent to the stretching vibration of O-H, reflecting the presence of hydroxyl group in PVA, and the distinctive apex at 831cm^{-1} is related to the bending vibration of C-H, reflecting the skeleton structure of PVA. The characteristic attains maximum 1018 cm^{-1} related to the stretching vibration of C-O-C and is

the glycosidic bond in chitosan molecule [42]. The characteristic attain maximum 3183cm-1 is N-H stretching vibration, while the C=C skeleton vibration peak at 1613 cm^{-1} indicates the presence of aromatic carbon skeleton in GO, and the epoxy group or hydroxyl group from GO shows C-O stretching vibration at 1047 cm-1. The distinctive apex at 3260 cm^{-1} corresponds to O-H stretching vibration, 2915 cm^{-1} matches to C-H stretching vibration, 1638 cm^{-1} equals to C=O stretching vibration, 1082 cm-1 and 827 cm-1 equals to C-O and C-H vibration, respectively [43]. The characteristics summit further verified the structural attributes of the PCG hydrogel containing PVA, GO and CS.

3.1.3. XRD analysis

As shown in Figure 3(b), PVA has an obvious diffraction peak near 2θ= 19°, which indicates that PVA has partial crystallization characteristics, and the crystallinity of PVA is affected by hydrogen bonding in its molecular structure. CS has a relatively wide diffraction attain maximum about 2θ = 20°, indicating that CS has a certain lacking a definite shape or form region at this position [44]. Chitosan has certain crystalline and amorphous properties, and the existence of amino and hydroxyl groups will form hydrogen bond networks, resulting in this wide peak on the XRD pattern. SiO_2 has a very wide peak, a characteristic that typically indicates that SiO_2 is amorphous silica, typically exhibiting a broad diffraction signal in the 2θ = 15° to 30° range. GO has a wide peak at about 2θ = 11°, which corresponds to the 001 face of GO. This diffraction peak usually reflects the layer spacing of graphene oxide, which is increased compared to graphite owing to the influence of functional groups containing oxygen. The width of the peaks also suggests that GO's amorphous nature is more pronounced. The X-ray diffraction pattern of PCG-SiO_2 shows a major diffraction maximum around 2θ = 22°, showing that the sample has some amorphous properties and may contain some ordered regions. This amorphous peak is usually associated with the presence of polymer matrix and amorphous silica, and the wider diffraction peak also indicates the amorphous nature of the material.

3.1.4. TG/DTG thermal stability analysis

FIG. 3(c) shows the thermogravimetric analytical graph. Within the temperature spectrum of ambient conditions to 500°C, PVA presents two significant weight loss stages, and about 10-15% weight loss occurs at 50-150 °C due to evaporation of water and low molecular weight volatiles. At 250-350℃ is the main decomposition stage of PVA, accompanied by a weight loss of about 60%, which is related to the degradation of PVA's skeleton structure. The weight loss of CS is about 10% due to the evaporation of adsorptive water in chitosan samples at 50-120 °C [45]. At 250-350 °C is its main thermal degradation stage, involving the cleavage of molecular chains and the disintegration of biological material, concluding in a weight loss of about 40%. PCG hydrogels showed a two-stage degradation trend similar to CS and PVA, while the weight loss curves of PCG showed improved stability of degradation relative to pure CS and PVA, possibly due to interactions between the different components. Compared to PCG hydrogels, the thermal stability of PCG-SiO_2 is improved, and this material exhibits relatively low weight loss in the high temperature region (250-500 °C), showing the introduction of silica improves the heat stability of the material. Figure 3(d) shows the thermogravimetric differential curve, where PVA has a significant peak weight loss rate at about 300°C. This indicates that the decomposition of PVA is the most intense at this temperature, which is the main decomposition stage. CS also has an obvious decomposition peak at about 300°C,

but the width of the peak is relatively narrow, indicating that the decomposition process is more concentrated. PCG hydrogels also have an obvious decomposition peak at about 300°C, but the peak is slightly to the right of CS and PVA, indicating that the degradation temperature of PCG hydrogels has increased, indicating that its thermal stability has improved. PCG-SiO_2 appears a decomposition peak in a similar temperature range (about 300-320°C), but the magnitude of the apex is small and slightly changed the right, indicating that PCG-SiO_2 decomposition speed is slower, and its thermal stability is further improved [46].

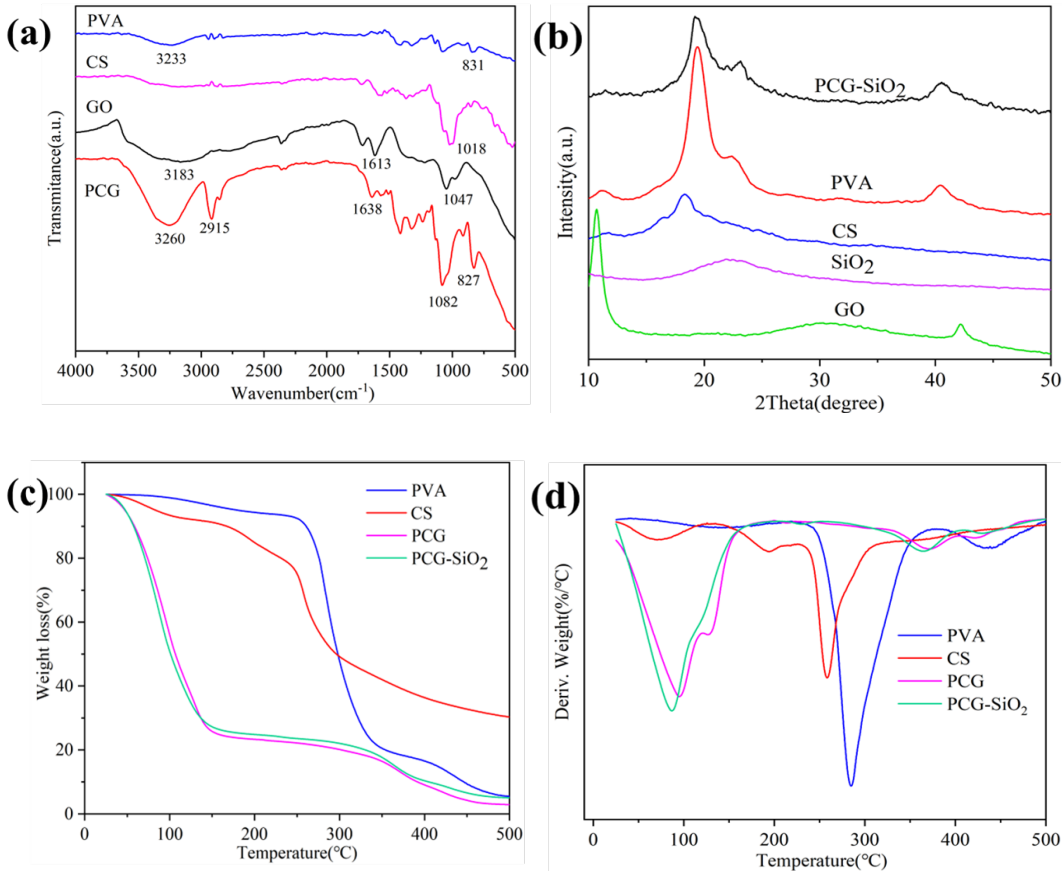

Fig. 3. (a) FTIR spectrum; (b) XRD spectrum; (c) TGA curve; (d) DTG curve.

3.2. Water content and swelling test analysis

Figure 4(a) shows the change of swelling ratio over time. Both PCG hydrogels and PCG-sio2 hydrogels show a trend of swelling ratio gradually escalating with the passage of time. The swelling ratio of PCG hydrogel is about 4.3, while the swelling ratio of PCG-sio2 is about 3.7, which indicates that the swelling capacity of PCG hydrogel is relatively higher. In the initial 20 hours, the swelling rate of the two hydrogels was identical, but with the extension of time, the swelling ratio of PCG hydrogels was larger than that of PCG-sio2 hydrogels. This may indicate that the introduction of SiO2 has an effect on the network structure of the hydrogel, reducing its water absorption capacity. Figure 4(b) shows the weight changes of the two hydrogels at various temporal intervals, reflecting the weight increase of the hydrogels after absorbing water. The weight of PCG hydrogels rose

rapidly with the increase of time, eventually reaching about 2.2g, while the weight of PCG-sio2 hydrogels leveled off at about 1.6g. This indicates that PCG hydrogels have a stronger water absorption capacity, while PCG-sio2 absorbs less water. This is consistent with the swelling ratio trend in Figure (a), indicating that the introduction of SiO2 reduces the swelling performance and water content of the hydrogel.

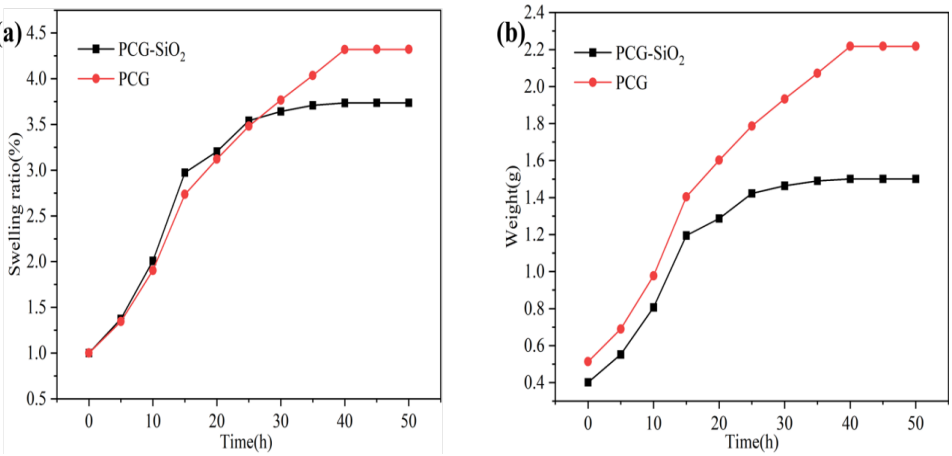

Fig. 4. (a) swelling performance curve; (b) water content curve.

3.3. Mechanical performance analysis

As can be seen from FIG. 5(e), increasing of strain, the stress also gradually increases, showing a non-linear upward trend. This shows that the two hydrogels exhibit obvious strain hardening properties under large compressive strain. In the whole strain range, the stress value of PCG-sio2 is slightly higher than that of PCG, especially when the strain reaches more than 60%, the stress rise of PCG-sio2 is more significant, and the maximum stress is close to 13000 kPa. This indicates that the introduction of SiO2 nanoparticles significantly improves the compression resistance of hydrogels. This is because SiO2 particles enhance the structural strength of the hydrogel, making it more stable during the compression process. It can be shown in FIG. 5(f) that in the lower strain range (about 0-150%), the stress of PCG increases linearly with the increase of strain, showing a typical elastic behavior. However, after reaching a certain strain, PCG quickly loses strength and breaks. This indicates that PCG has limited ductility and is prone to fracture when the tensile strain is large. However, the mechanical characteristics of PCG-SiO2 samples are significantly improved after the introduction of different contents of SiO2 particles. Specifically, the stress-strain curves of PCG-sio2 (1) and PCG-sio2 (2) have higher fracture strain than those of PCG, indicating that the introduction of a little quantity of SiO2 is helpful to increase the ductility and strength of hydrogels. PCG-SiO2(3) shows the highest fracture strain and fracture stress, with a maximum strain of about 300% and a maximum stress of nearly 2000 kPa. This indicates that the higher content of SiO2 makes the hydrogel have stronger fracture resistance during the stretching process, indicating that its enhancement effect is significant.

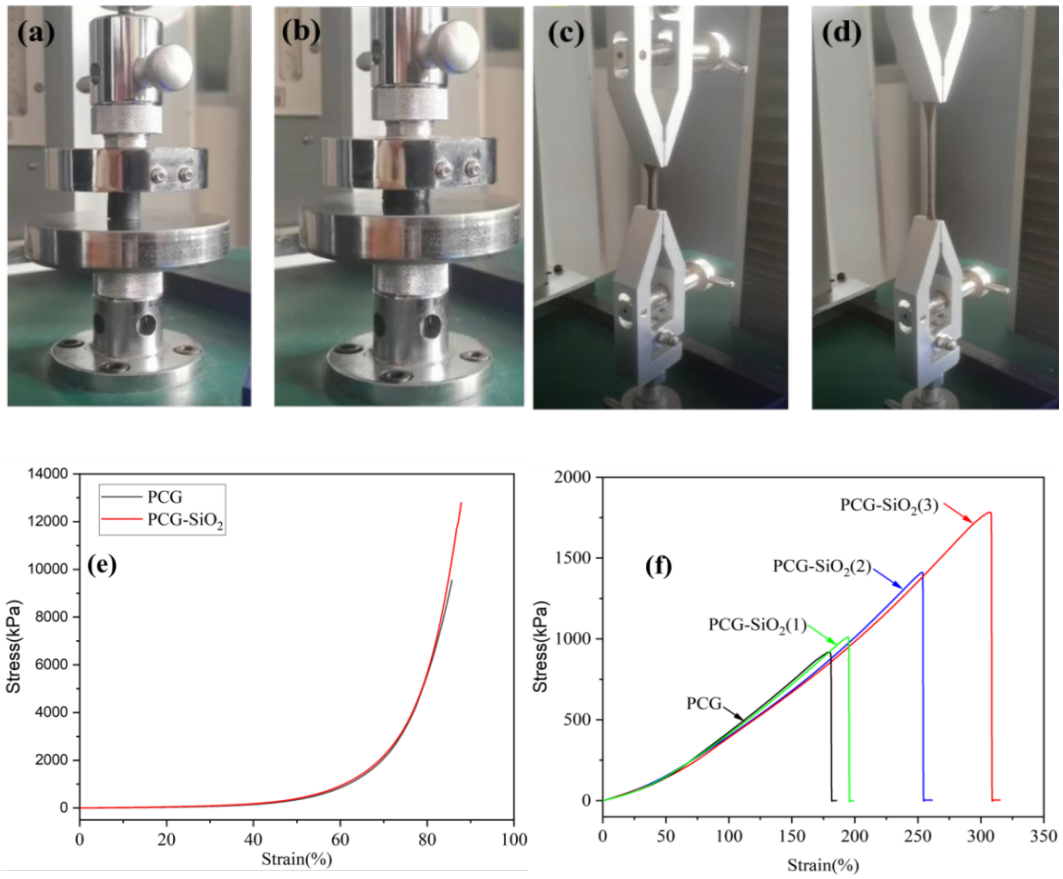

Fig. 5. (a) (b) Schematic diagram of compression test; (c) (d) Schematic diagram of tensile test; (e) Compression curve; (f) Tensile curve.

3.4 Adsorption performance analysis

3.4.1. Influence of initial concentration of methylene blue

As shown in Figure 6, the absorption peaks of all spectra are located at about 650 nm, which is the characteristic absorption peak of methylene blue, indicating that hydrogel has adsorption effect on methylene blue. With the increase of sample number from 1 to 5, the absorbance gradually decreased, indicating that the adsorption capacity of hydrogel to methylene blue gradually decreased, and the intensity of absorption peak was related to the concentration of methylene blue dye[47-48]. A higher absorbance means that the dye concentration is higher, indicating that the corresponding sample has more dye residue. Figure (a) to Figure (d) shows that the overall absorbance increases with the increase of the initial dye concentration, which indicates that the residual dye concentration after hydrogel adsorption is higher when the initial dye volume is larger, indicating that the adsorption effect is affected by the amount of dye. With the increase of the initial dye concentration (from 5 ml to 20 ml), the adsorption capacity of the hydrogel is gradually weakened, which may be because the adsorption site of the hydrogel is limited, and the dye amount is increased, and it is not completely adsorbed. The absorbance values marked in the figure (0.18, 1.51, 2.82, 3.02) reflect the concentration of residual dyes at different volumes. From these values, it is obvious that with the increase of initial dye volume, the absorbance increases, and the adsorption efficiency of hydrogel decreases.

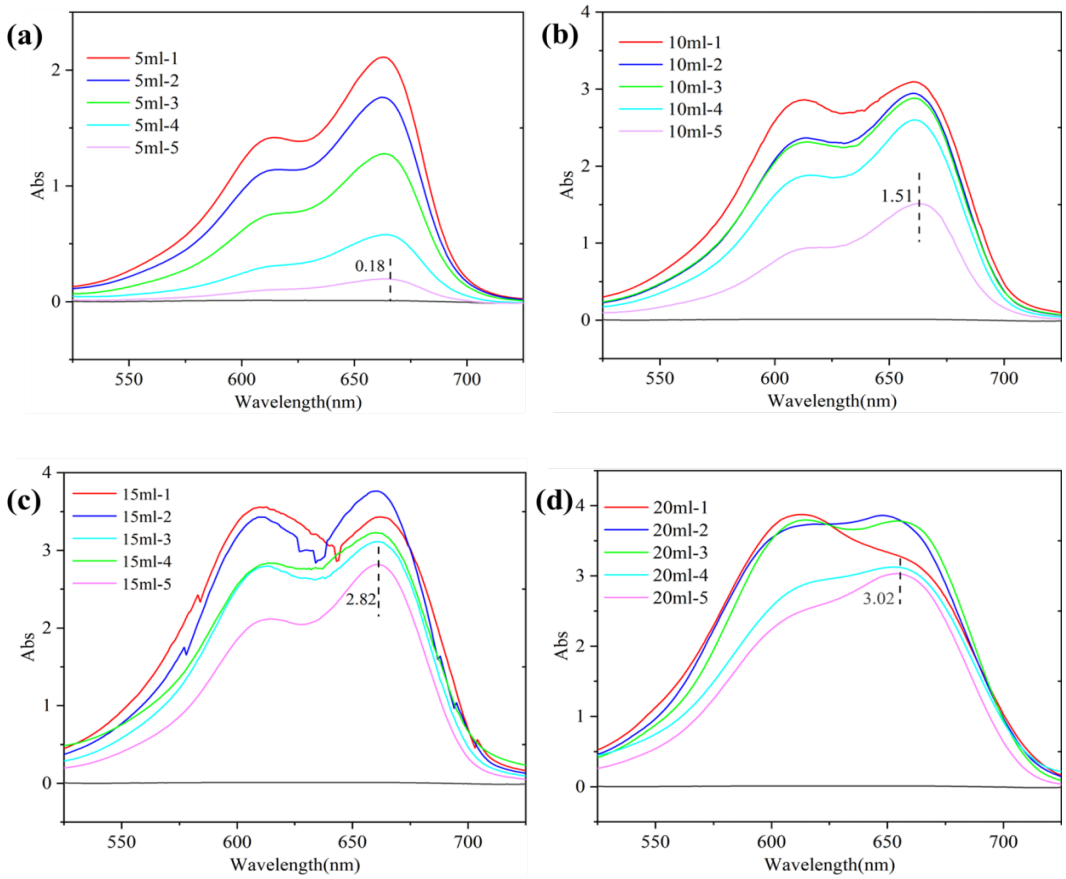

Fig. 6. UV-visible spectra of supernatants after adsorption of methylene blue wastewater dye at different concentrations.

3.4.2. The effect of temperature

As shown in Figure 7, with the increase of temperature, the absorbance gradually decreased, indicating that PCG hydrogel enhanced the methylene blue adsorption effect under high temperature conditions. Specific analysis of FIG. 8(a) to FIG. 8(d): At 20°C, the higher absorbance reached 2.38, indicating that the residual dye concentration was higher at this temperature; At 35°C, the absorbance decreased to 1.62, indicating that the adsorption effect was improved. When the temperature is elevated to 50°C, the absorbance is further reduced to 0.87, and the adsorption effect is obviously enhanced. At 65°C, the absorbance is 0.94, which is close to 50°C, and the adsorption effect also reaches a higher level, but it is slightly reduced compared with 50°C. As the temperature rises, the kinetic energy of the molecules escalates, which may help the methylene blue molecules to disperse more quickly into the inside of the hydrogel, improving the adsorption efficiency. However, the adsorption effect of 65°C is similar to that of 50°C, indicating that under high temperature conditions, the adsorption capacity of hydrogel may tend to be saturated or the adsorption kinetics may change due to high temperature, thus slightly reducing the adsorption effect. Therefore, PCG hydrogels exhibit better adsorption capacity at appropriate high temperatures (50°C).

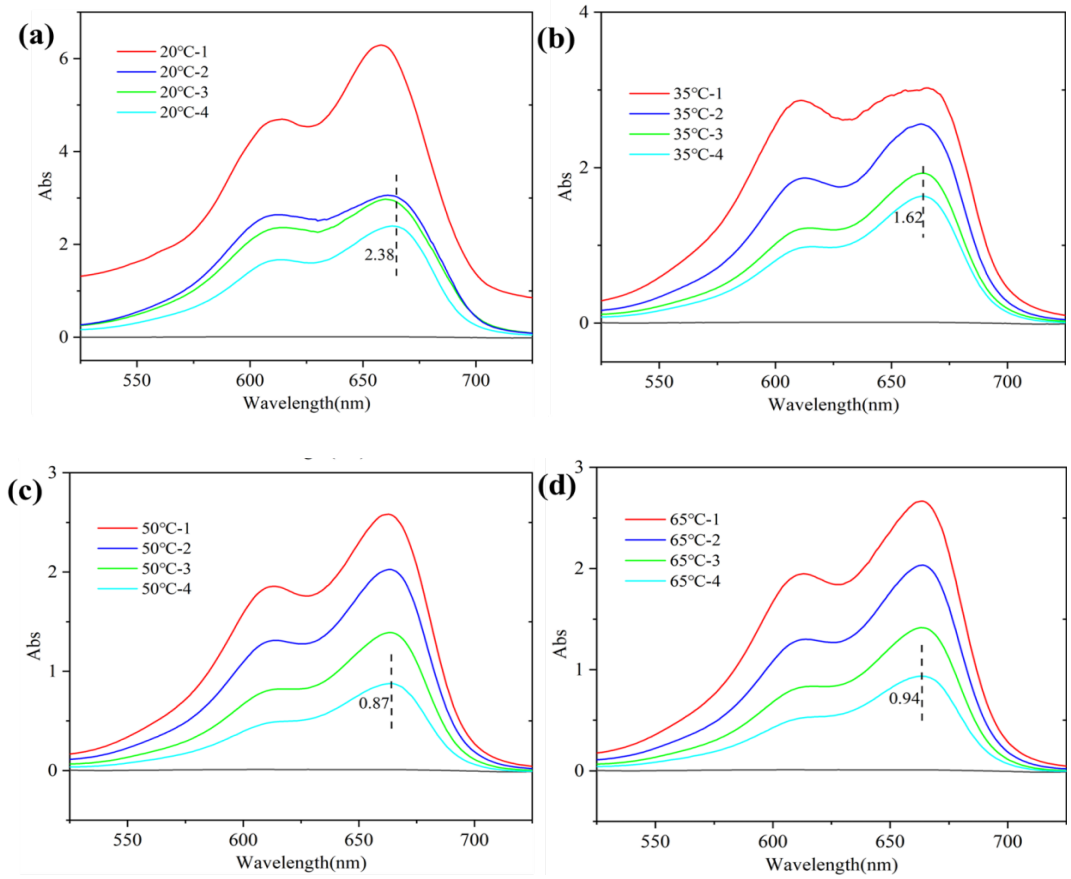

Fig. 7. UV-visible spectra of supernatant after adsorption of dye from wastewater at different temperatures.

3.4.3. Influence of PH

As shown in Figure 8, under the condition of pH= 4, the absorbance is 2.66, indicating that the adsorption effect is relatively poor under this pH condition, and the dye residue concentration is high. Under the condition of pH= 6, the absorbance is 2.35, which is lower than pH 4, and the adsorption effect is improved. Under the condition of pH= 7, the absorbance is 2.11, and the adsorption effect continues to improve. Under the condition of pH= 8, the absorbance increases to 2.85, which shows that the adsorption effect of pH 8 is not increase compared with pH 6 and pH 7. Between pH= 4 and pH= 7, the adsorption effect gradually becomes better. This is owing to the effect of pH on the surface charge of the hydrogel and the ionic state of methylene blue molecules. In a neutral or weakly alkaline environment, methylene blue is more likely to bind to the exterior of the hydrogel, enhancing the adsorption efficacy. The increase in absorbance at pH= 8 May be owing to changes in the structure or surface charge of the hydrogel under strong alkaline conditions, which affect the effectiveness of the adsorption site, leading to a reduction in the adsorption efficacy.

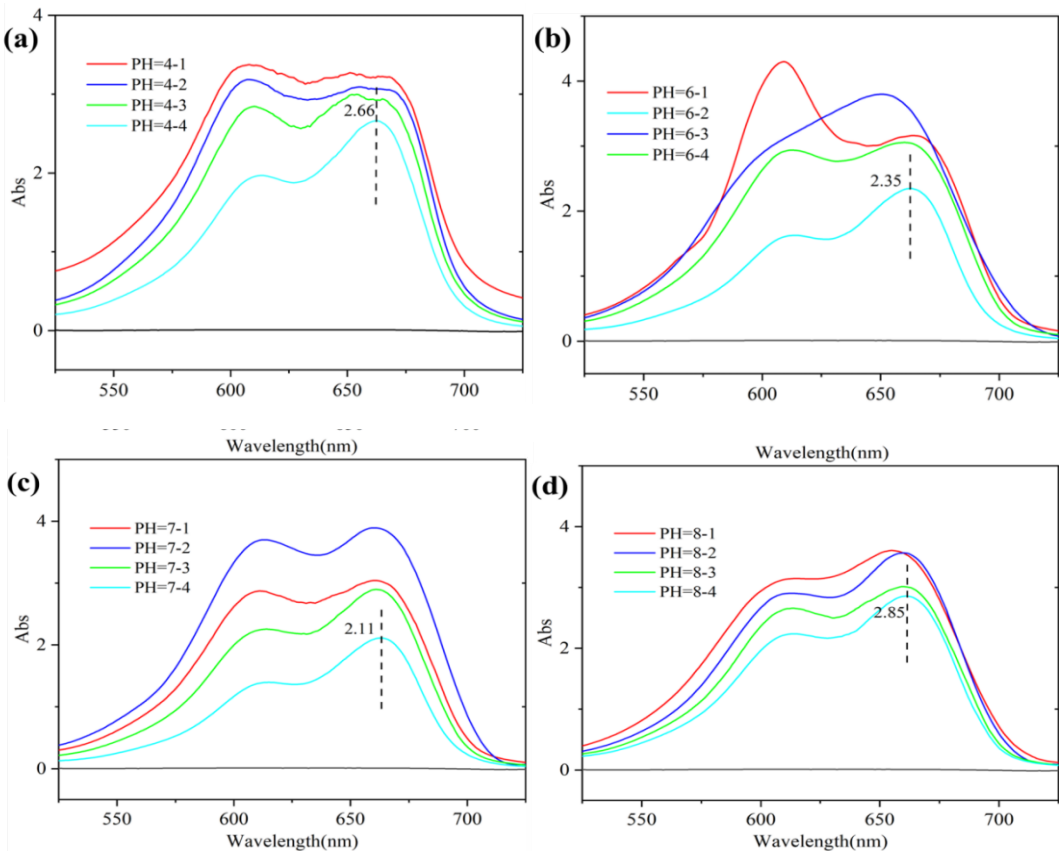

Fig. 8. UV-visible spectra of supernatant after adsorption of dye in wastewater at different PH.

3.4.4. Influence of adsorbent

As shown in Figure 9(a), the lowest absorbance is 0.08, indicating that the chitosan-based hydrogel has a good adsorption effect on methylene blue. The CS gradients in hydrogels were different, but the absorbance of aqueous solution changed little after adsorption, indicating that chitosan-based hydrogels showed stability in terms of adsorption properties, which was related to the interaction of amino groups of chitosan and molecules of methylene blue. The absorbance shown in Figure 10(b) is relatively high, reaching a maximum of more than 3.0, but with the increase of the proportion of graphene oxide, the lowest absorbance also reached 0.26, and the adsorption efficacy of the hydrogel was significantly enhanced. Because GO has a extensive specific surface area and plentiful oxygen functional groups, it is helpful to adsorb methylene blue molecules, but its adsorption performance is still not as significant as that of chitosan-based hydrogels. Therefore, in the case of CS as the main adsorbent, increasing the proportion of GO at the same time can further improve the adsorption capacity.

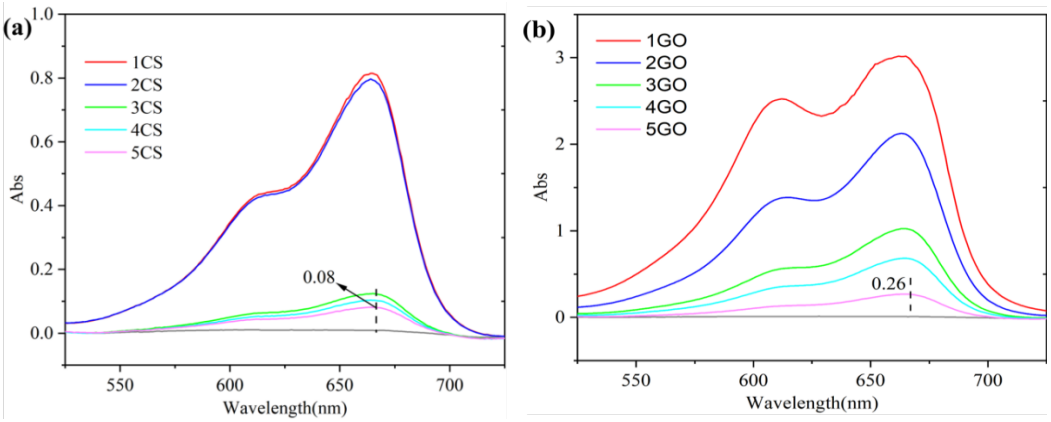

Fig. 9. UV-visible spectra of supernatants from hydrogels with different CS and GO contents after adsorption of wastewater dye.

3.5. Adsorption kinetics analysis

3.5.1. Adsorption performance under 50℃ conditions

The fitting results of the PCG hydrogel pseudo-first-order kinetic model are displayed in FIG. 10(a), whose R2 is 0.9259, indicating a high degree of fitting and a week adsorption content of 50mg/g, showing in Table 1. According to this linear regression results, the pseudo-first-order dynamic framework can partially clarify the adsorption process, and the fitting shows the initial adsorption stage is predominantly governed by the physical interaction, and the adsorption rate is faster in an early period and then gradually becomes stable, but the pseudo-first-order dynamic framework is not the only control mechanism. FIG. 10(b) shows the fitting outcomes of the framework of pseudo-second-order, whose R2 is 9848.Different in the framework of pseudo-first-order, the framework of pseudo-second-order shows a better linear correlation, demonstrating that the model more accurately characterises the adsorption mechanism of methylene blue by PCG hydrogel. the framework of pseudo-second-order fits well, indicating that adsorption process is predominantly governed by chemisorption, involving the formation of chemical bonds and electron exchange, and its saturation adsorption performance is up to 259mg/g, which is more than five times that of the pseudo-first-order saturation adsorption.

Table S1. Kinetic parameters of MB adsorption by the PCG hydrogel at 50℃.

Kinetic model	Parameters	Value
pseudo-first-order kinetics	k1 (L· mg-1)	-6.16*10-4
	qe1 (mg· g-1)	50
	R2	0.9259
pseudo-second-order kinetics	k2 (L· mg-1)	0.0079
	qe2 (mg· g1)	259
	R2	0.9848

3.5.2. Adsorption performance under PH=7 conditions

FIG. 11(b) From the linear regression results, the framework of pseudo-second-order can partially clarify the adsorption process, and the initial adsorption stage is controlled by chemical interaction, but this may not be the only mechanism controlling the entire adsorption process. Its R2 is 0.9276, and the saturation adsorption energy is 65mg/g, as shown in Table 2. Figure 11(a) shows the fitting results of the pseudo-first-order kinetic model, whose R2 is 0.9779, indicating that the pseudo-first-order model exhibits stronger linear correlation, and its saturation adsorption performance is up to 267mg/g, as shown in Table 2, which further proves that it is more consistent with the pseudo-first-order framework. This framework better clarify the adsorption process of methylene blue by PCG hydrogel. The high linearity indicates that the adsorption process is predominantly governed by physical adsorption., possibly because the network structure of PCG hydrogels is destroyed in the over acid or alkaline environment.

Table S2. Kinetic parameters of MB adsorption by the PCG hydrogel at PH=7.

Kinetic model	Parameters	Value
pseudo-first-order kinetics	k1 (L· mg-1)	-4.0*10-4
	qe1 (mg· g-1)	267
	R2	0.9779
pseudo-second-order kinetics	k2 (L· mg-1)	0.0043
	qe2 (mg· g1)	65
	R2	0.9276

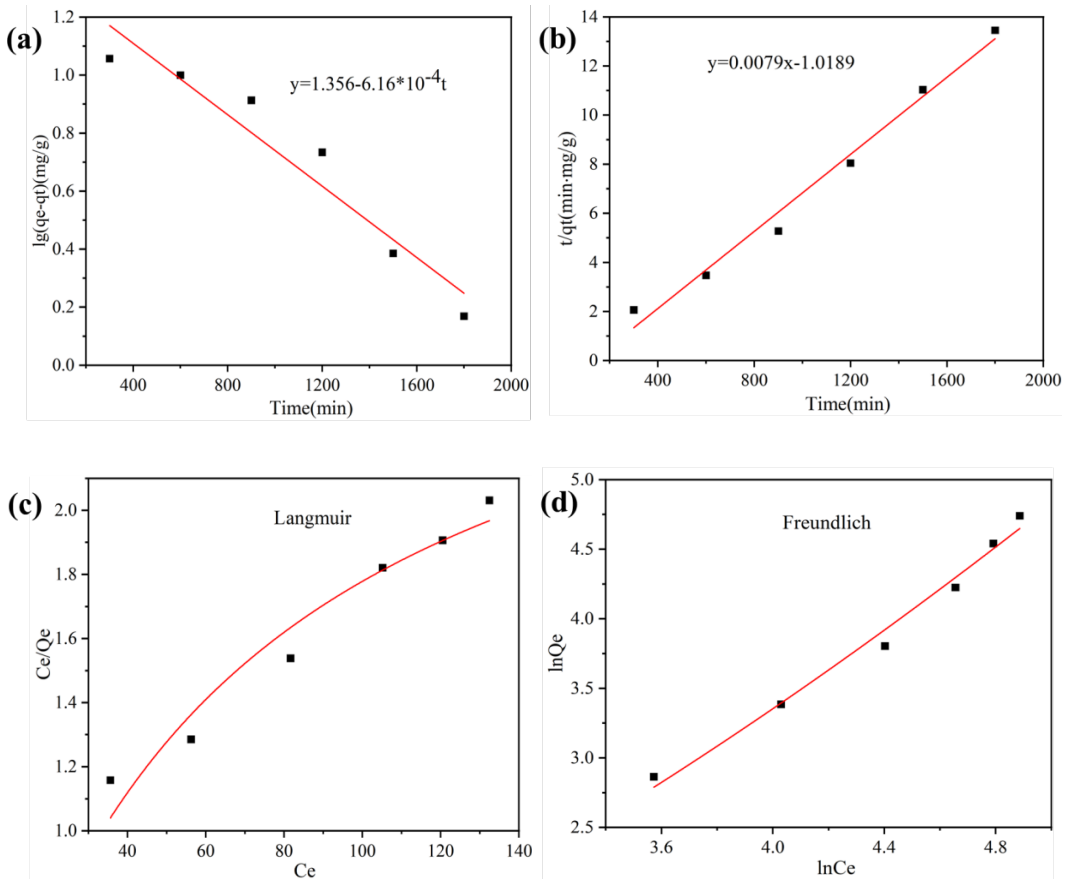

Fig. 10. At 50℃; (a) first-order adsorption kinetics; (b) second-order adsorption kinetics; (c) Langmuir isothermal adsorption model; (d) Freundlich isothermal adsorption model.

3.6. Isothermal model analysis

3.6.1. Isothermal adsorption at 50°C

Figure 10(c) shows the fitting of the Langmuir isotherm model, which assumes that adsorption transpires on a homogeneous surface where each adsorption site possesses similar adsorption energy. From the optimal outcomes in Table 3, it can be seen that the R^2 is 0.9469, the saturation adsorption concentration reaches 491 mg/g, the Langmuir model can accurately elucidate the adsorption characteristics of PCG hydrogel for methylene blue, indicating that the adsorption process exhibits monolayer adsorption behavior and there is no significant interplay between different adsorption sites. Figure 11(d) shows the application of the Freundlich isotherm model, and Table 3 results show its R2 is 0.9865, higher than the Langmuir model, indicating that the Freundlich model exhibits better fitting, suggesting that the adsorption of PCG hydrogel is more influenced by multilayer adsorption and there are adsorption sites with different energies on the surface. This indicates that the adsorption process is not entirely uniform, with multiple adsorption sites having different adsorption energies, and the adsorption capacity increases with increasing concentration.

Table S3. Isothermal adsorption model parameters of PCG hydrogel adsorbing MB at 50°C.

Model	Parameters	Value
Langmuir isotherm	KL (L· mg-1)	2.9273
	qm (mg· g-1)	491
	R2	0.9469
Freundlich isotherm	KF (L· mg-1)	47
	n	0.35
	R2	0.9865

3.6.2. Isothermal adsorption at PH=8

The Langmuir isotherm model, which asserts that adsorption occurs on a uniform surface and that each adsorption site has the same adsorption energy, fits data as shown in Figure 10(c). According to the fitting results in Table 3, its R2 is 0.9469, and the saturation adsorption concentration reaches 491 mg/g. Langmuir model can describe the adsorption behavior of PCG hydrogel on methylene blue, indicating that the adsorption process has a single molecular layer adsorption behavior, and there is no obvious interaction between adsorption sites. Figure 10(d) shows the application of the Freundlich isotherm model. The results in Table 3 show that the R2 of the Freundlich model is 0.9865, which is higher than the Langmuir model. Therefore, the Freundlich model shows a better fitting degree, indicating that the adsorption of PCG hydrogel is more affected by multi-layer adsorption. There are different energy adsorption sites on the surface. This indicates that the adsorption process is not completely uniform, there may be multiple adsorption sites with different adsorption energies, and the adsorption capacity escalates with rising concentration.

Table S4. Isothermal adsorption model parameters of PCG hydrogel adsorbing MB at PH=7.

Model	Parameters	Value
Langmuir isotherm	KL (L· mg-1)	2.9597
	qm (mg· g-1)	328
	R2	0.8899
Freundlich isotherm	KF (L· mg-1)	56
	n	0.68
	R2	0.9205

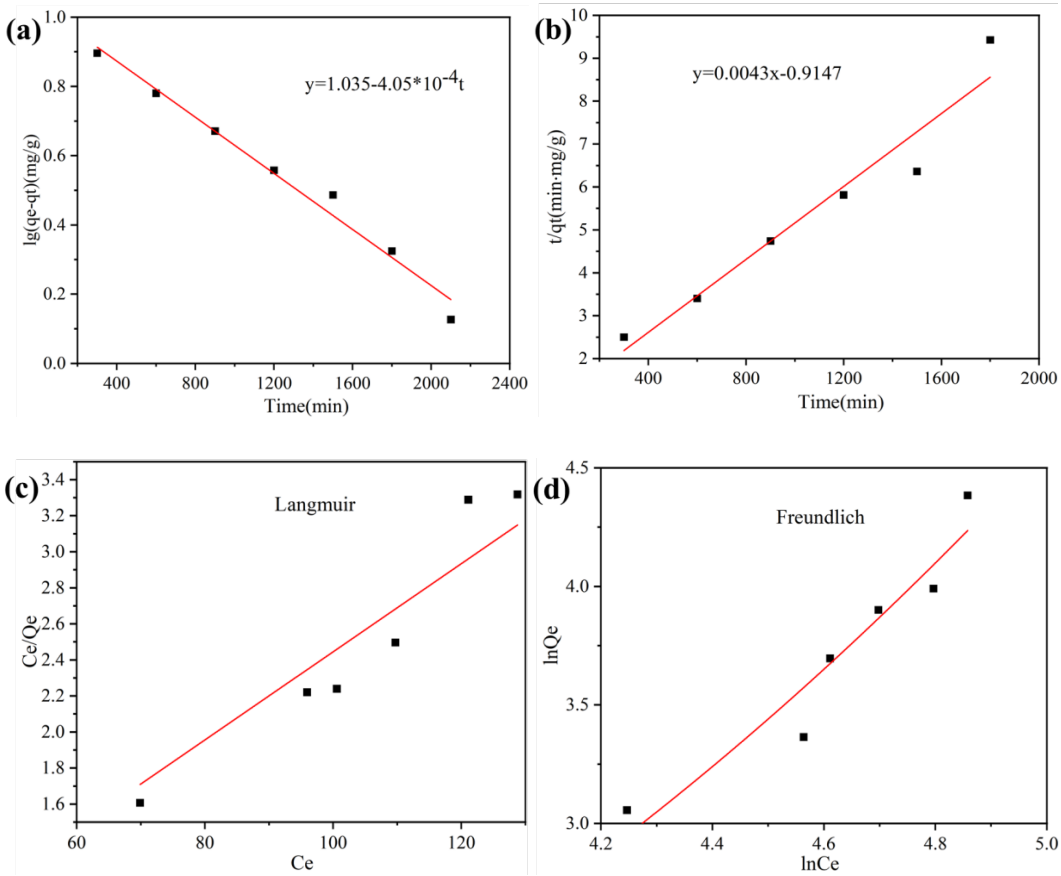

Fig. 11. Shows the first-order adsorption kinetics (a), second-order adsorption kinetics (b), Langmuir isothermal adsorption model (c) and Freundlich isothermal adsorption model (d) at PH=7.

3.7. Adsorption mechanism analysis

PCG hydrogel has both physical adsorption process, and chemical adsorption process in the process of the blue adsorption of methylene, and the combination of the two makes the adsorption performance of PCG hydrogel reach the maximum. Physical adsorption: The porous structure in the composite hydrogel provides a substantial quantity of adsorption sites, facilitating the diffusion and storage of dye molecules within the material. The dimensions and configuration of the pores are very favorable for the diffusion of methylene blue, which can increase the duration of residence the

molecules inside the hydrogel, thereby increasing the adsorption efficiency. Chemical adsorption: The surface functional groups, including hydroxyl and carboxyl groups of nanoscale graphene oxide can be bonded to methylene blue molecules through hydrogen bonding or electrostatic interactions. The negative charge present on the surface of graphene oxide forms electrostatic adsorption with a cationic dye, methylene blue In addition, the π-π involving between the aromatic structure of GO and the fragrant ring of methylene blue also helps to further fix the dye molecules. The addition of nano-hydrophilic silica may further enhance the mechanical properties and adsorption properties of hydrogels. The high specific surface area of silica helps to provide more adsorption sites, while its hydrophilicity facilitates the expansion of hydrogels in the aqueous phase and the diffusion of dye molecules.

As shown in Figure 12, Figure a and Figure e are the full spectrum of PCG hydrogel before and after adsorption. By comparison, the hydrogel figure a before adsorption shows the peaks of C1s, O 1s and Si 2p, and the sources of these elements are polyvinyl alcohol, chitosan, graphene oxide and nano-silica. After adsorption (Figure e), the elements shown in the full spectrum did not change much, and were still dominated by C1s, O 1s and Si 2p, but some subtle changes could be seen, such as the intensity of the absorption peak was different, indicating that some changes had occurred in the chemical environment during the adsorption process. In Figure b, the C1s peak is decomposed into three sub-peaks, corresponding to C-C (carbon-carbon bond), C-O (carbon-oxygen bond) and C=O (carbon-oxygen double bond), respectively. After adsorption of methylene blue, the peak intensity and relative proportion of C1s in Figure f change, and the peak of C=O is relatively enhanced, indicating that some oxidation or chemical binding changes occur during the adsorption process. This is associated with the molecular structure of methylene blue. In Figure c, the O-1s peak mainly corresponds to the C-O bond, which is mainly derived from the hydroxyl group in polyvinyl alcohol and chitosan; The shape and relative intensity of O1s peak in Figure g changed after adsorption of methylene blue, indicating that the oxygen environment in oxides and organic compounds had changed to some extent. These changes reflect the interaction of thioblue bonds in methylene blue molecules with hydroxyl groups or other functional groups in the hydrogel. The Si2p peak in corresponds to the Si-O bond and is derived from hydrophilic nanosilica. After adsorption of methylene blue (FIG. h), the intensity and peak position of Si 2p peak did not change significantly, indicating that the chemical environment of silicon element remained relatively stable, indicating that there was no obvious chemical reaction between nano silica and methylene blue directly. After adsorption of methylene blue, the peak intensity and relative ratio of C1s and O1s changed significantly, indicating that the adsorption of methylene blue mainly affected the chemical environment of carbon and oxygen elements in the hydrogel, especially the change of hydroxyl group and carbon-oxygen double bond. The Si2p peak remained basically unchanged, indicating that the role of nano silica as an inorganic enhancement phase is more physical adsorption than chemical reaction with dye molecules.

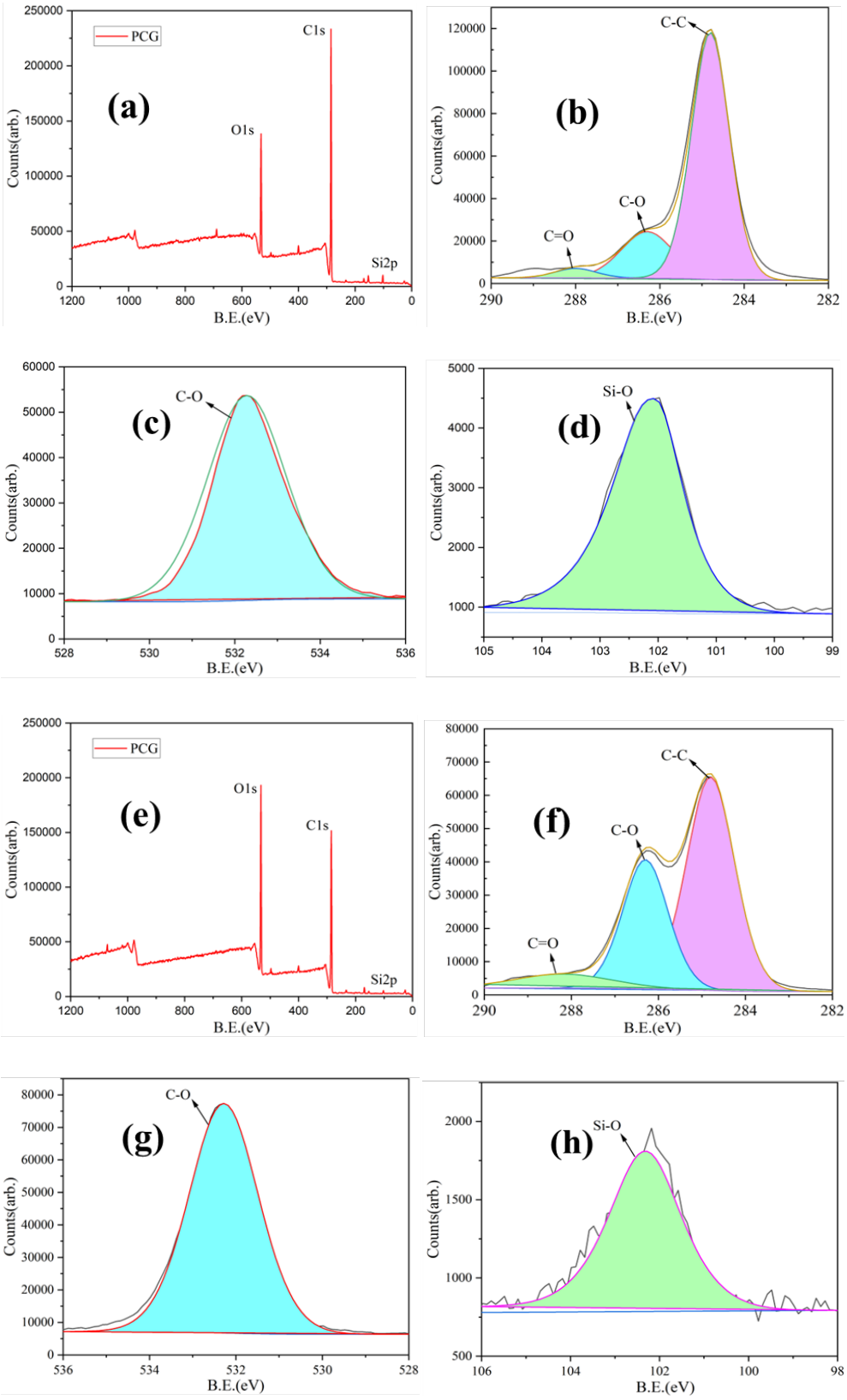

Fig. 12. (a)-(d) XPS spectra of PCG hydrogel before adsorption;
(e)-(h) XPS spectra of PcG hydrogel after adsorption.

4. Conclusion

This paper examines a composite hydrogel consisting of polyvinyl alcohol, chitosan, hydrophilic silica and graphene oxide with high mechanical properties, porous structure and excellent adsorption properties was prepared by physical crosslinking of freeze-thawing method, which can effectively adsorb methylene blue in dye wastewater. The addition of chitosan to the PVA skeleton can enhance the adsorption efficacy of PVA hydrogels, but also increase the stability of chitosan hydrogels. On this basis, the introduction of hydrophilic nano-silica and graphene oxide can significantly enhance the mechanical integrity of PPG three-dimensional network structure composite hydrogels. The tensile strength, compressive strength and tensile length properties of the composite hydrogel have been markedly enhanced. Tensile and compression tests show that the maximum tensile strength of the composite hydrogel is 2000kPa, the maximum tensile displacement exceeds 300% of the initial form, and the maximum compressive strength is up to 13000kPa, which proves its excellent mechanical properties. The effects of initial solution concentration, temperature, PH, GO content (i.e., adsorbent concentration) and chitosan content on the adsorption properties were also discussed. The study showed that the optimal adsorption temperature was 50℃, the ideal adsorption pH was 7.0, and the optimal adsorbent concentration was 5%. Adsorption kinetics model was employed to model the adsorption rate of the hydrogel, and it was concluded that the fitting was more consistent with the physical adsorption process at 50℃, and more consistent with chemisorption at pH=7.0. At the same time, the isothermal adsorption model is used to explore not only the single-layer adsorption and multi-layer adsorption of hydrogels, but also the physicochemical adsorption. The composite processing of 3D network structure composite hydrogels or even multi-dimensional network structure composite hydrogels will become a new strategy to improve conventional hydrogels, which is practical, cheap and environmentally friendly, and has broad prospects in industrial applications.

References

[1] M. Haseena, M. Faheem Malik, A. Javed, S. Arshad, N. Asif, S. Zulfiqar, J. Hanif, Environ. Risk Assess. Remediat. 01 (2017) 16-19; https://doi.org/10.4066/2529-8046.100020

[2] Z. Wu, W. Huang, X. Shan, Z. Li, Int. J. Biol. Macromol. 143 (2020) 325-333; https://doi.org/10.1016/j.ijbiomac.2019.12.017

[3] L.M.S. de Farias, M.G. Ghislandi, M.F. de Aguiar, D.B.R.S. Silva, A.N.R. Leal, F. De A.O. Silva, T.J.M. Fraga, C.P. De Melo, K.G.B. Alves, Mater. Chem. Phys. 276 (2022), 125356; https://doi.org/10.1016/j.matchemphys.2021.125356

[4] A.A. Al-Gheethi, Q.M. Azhar, P. Senthil Kumar, A.A. Yusuf, A.K. Al-Buriahi, R.M. S. Radin Mohamed, M.M. Al-Shaibani, Chemosphere 287 (2022), 132080; https://doi.org/10.1016/j.chemosphere.2021.132080

[5] H. Asadzadeh Patehkhor, M. Fattahi, M. Khosravi-Nikou, Sci. Rep. 11 (2021) 24177; https://doi.org/10.1038/s41598-021-03492-5

[6] H. Yuan, J. Peng, T. Ren, Q. Luo, Y. Luo, N. Zhang, Y. Huang, X. Guo, Y. Wu, Sci. Total Environ. 760 (2021), 143395; https://doi.org/10.1016/j.scitotenv.2020.143395

[7] K. He, G. Chen, G. Zeng, A. Chen, Z. Huang, J. Shi, T. Huang, M. Peng, L. Hu, Appl. Catal. B Environ. 228 (2018) 19-28; https://doi.org/10.1016/j.apcatb.2018.01.061

[8] P. Xiao, P. Wang, H. Li, Q. Li, Y. Shi, X.L. Wu, H. Lin, J. Chen, X. Wang, J. Hazard. Mater. 345 (2018) 123-130; https://doi.org/10.1016/j.jhazmat.2017.11.001

[9] J. Kang, H. Zhang, X. Duan, H. Sun, X. Tan, S. Liu, S. Wang, Chem. Eng. J. 362 (2019) 251-261; https://doi.org/10.1016/j.cej.2019.01.035

[10] A. Daas, O. Hamdaoui, J. Hazard. Mater. 178 (2010) 973-981; https://doi.org/10.1016/j.jhazmat.2010.02.033

[11] L. Liu, Z. Chen, J. Zhang, D. Shan, Y. Wu, L. Bai, B. Wang, J. Water Process Eng. 42 (2021), 102122; https://doi.org/10.1016/j.jwpe.2021.102122

[12] J. Zhang, Y. Ma, W. Zhang, X. Huang, X. Wang, Y. Huang, P. Zhang, J. Clean. Prod. 365 (2022), 132810; https://doi.org/10.1016/j.jclepro.2022.132810

[13] L. Zhang, L. Dai, X. Li, W. Yu, S. Li, J. Guan, New J. Chem. 46 (2022) 2272-2281; https://doi.org/10.1039/D1NJ05395G

[14] P.J.N. Kottam, Inorg. Chem. Commun. 125 (2021), 108460; https://doi.org/10.1016/j.inoche.2021.108460

[15] T.P. Chou, Q. Zhang, G. Cao, J. Phys. Chem. C 111 (2007) 18804-18811; https://doi.org/10.1021/jp076724f

[16] Isha Dogra, Bheema Rajesh Kumar, Krishna C. Etika, Chavali Murthy, Amany Salah Khalifa, Amal F. Gharib, ElAskary Ahmad, J. King Saud Univ. Sci. 34 (2022), 102122; https://doi.org/10.1016/j.jksus.2022.102122

[17] Humaira Seema, Nadia Khan, Anwar ul Haq Ali Shah, Amir Muhammad, Mater. Chem. Phys. 306 (2023), 128003; https://doi.org/10.1016/j.matchemphys.2023.128003

[18] Lele Chen, Liu Zhao, Jipeng Shi, Chengbo Wang, Ling Ding, Xu Ding, Guixiang Teng, Jianping Wu, Ji Zhang, Process Biochem. 122 (2022) 13-28; https://doi.org/10.1016/j.procbio.2022.08.025

[19] F.O. Gokmen, E. Yaman, S. Temel, Microchem. J. 168 (2021), 106357; https://doi.org/10.1016/j.microc.2021.106357

[20] Athmar K. Al-shammari, Ehssan Al-Bermany, J. Polym. Res. 29 (2022) 351; https://doi.org/10.1007/s10965-022-03210-3

[21] Yamei Liu, Caili Hou, Tifeng Jiao, Jingwen Song, Xu Zhang, Ruirui Xing, Jingxin Zhou, Lexin Zhang, Qiuming Peng, Nanomaterials 8 (2018) 35; https://doi.org/10.3390/nano8010035

[22] Wenjia Kong, Qinyan Yue, Li Qian, Baoyu Gao, Sci. Total Environ. 668 (2019) 1165-1174; https://doi.org/10.1016/j.scitotenv.2019.03.095

[23] Lv Chang, Huafeng Tian, Xing Zhang, Aimin Xiang, Polym. Test. 70 (2018) 67-72; https://doi.org/10.1016/j.polymertesting.2018.06.024

[24] S. Prabhu, L. Cindrella, Oh Joong Kwon, K. Mohanraju, Sol. Energy Mater. Sol. Cell. 169 (2017) 304-312; https://doi.org/10.1016/j.solmat.2017.05.023

[25] Manxi Sun, Jianhui Qiu, Shuping Jin, Hongjian Huang, Wendi Liu, Eiichi Sakai, Ji Lei, Polym. Bull. 78 (2021) 7183-7198; https://doi.org/10.1007/s00289-020-03462-3

[26] Niladri Sarkar, Gyanaranjan Sahoo, K. Sarat, Swain, Mater. Chem. Phys. 250 (2020),

123022; https://doi.org/10.1016/j.matchemphys.2020.123022

[27] M.L. Pita-Lopez, ' G. Fletes-Vargas, H. Espinosa-Andrews, R. Rodríguez-Rodríguez, Eur. Polym. J. 145 (2021) 110176; https://doi.org/10.1016/j.eurpolymj.2020.110176

[28] Ahmed M. Elgarahy, M.G. Eloffy, Eric Guibal, Huda M. Alghamdi, Khalid Z. Elwakeel, Chin. J. Chem. Eng. 64 (2023) 292-320; https://doi.org/10.1016/j.cjche.2023.05.018

[29] Y. Chena, X. Yana, J. Zhaoa, H. Fenga, P. Lib, Z. Tonga, Z. Yanga, S. Lic, J. Yanga, S. Ji, Carbohydr. Polym. 191 (2018) 8-16; https://doi.org/10.1016/j.carbpol.2018.02.065

[30] H.-S. Kang, S.-H. Park, Y.-G. Lee, T.-I. Son, J. Appl. Polym. Sci. 103 (2007) 386-394; https://doi.org/10.1002/app.24623

[31] Y. Luo, Q. Wang, Int. J. Biol. Macromol. 64 (2014) 353-367; https://doi.org/10.1016/j.ijbiomac.2013.12.017

[32] A. 'Ciri'c, J. Milinkovi'c Budinˇci'c, Đ. Medarevi'c, V. Dobriˇci'c, M. Rmandi'c, T. Barudˇzija, A. Malenovi'c, L. Petrovi'c, L. Djekic, Int. J. Biol. Macromol. 221 (2022) 48-60; https://doi.org/10.1016/j.ijbiomac.2022.08.190

[33] T.S. Anirudhan, Sekhar V. Chithra, Syam S. Nair, J. Drug Deliv. Sci. Technol. 51 (2019) 569-582; https://doi.org/10.1016/j.jddst.2019.03.036

[34] J. Patel, B. Maji, N.S. Hari Narayana Moorthya, S. Maiti, RSC Adv. 10 (2020) 27103; https://doi.org/10.1039/D0RA04366D

[35] X. Fu, F. Qin, T. Liu, X. Zhang, Energy Fuel 36 (1) (2022) 181-194; https://doi.org/10.1021/acs.energyfuels.1c02941

[36] B. Katzbauer, Polym. Degrad. Stab. 59 (1998) 81-84; https://doi.org/10.1016/S0141-3910(97)00180-8

[37] H. Yeon Jang, K. Zhang, B. Hyun Chon, H. Jin Choi, J. Ind. Eng. Chem. 21 (2015) 741-745; https://doi.org/10.1016/j.jiec.2014.04.005

[38] S. Kou, L. Peters, M. Mucalo, Carbohydr. Polym. 282 (2022) 119132; https://doi.org/10.1016/j.carbpol.2022.119132

[39] M. Hosseinnejada, S. Mahdi Jafari, Int. J. Biol. Macromol. 85 (2016) 467-475; https://doi.org/10.1016/j.ijbiomac.2016.01.022

[40] V. Dhopeshwarkar, Joel L. Zatz, Drug Dev. Ind. Pharm. 19 (9) (2008) 999-1017; https://doi.org/10.3109/03639049309062997

[41] M. Fu Lu, L. Woodward, S. Borodkin, Drug Dev. Ind. Pharm. 17 (14) (2004) 1987-2004; https://doi.org/10.3109/03639049109048063

[42] M.-A. Archer, K. Ofori-Kwakye, N. Kuntworbe, M. Aduenimaa Bonsu, Int. J. Pharm. Technol. 9 (7) (2016) 369-380.

[43] J. Fan, K. Wang, M. Liu, Z. He, Carbohydr. Polym. 73 (2) (2008) 241-247; https://doi.org/10.1016/j.carbpol.2007.11.027

[44]S.Alavi,S.Alireza Mortazavi, Iran, J. Pharm. Res. 17 (4) (2018) 1172-1181.

[45] X.Hua,Y.Wanga, L. Zhanga, M. Xua, Carbohydr. Polym. 234 (2020) 115920; https://doi.org/10.1016/j.carbpol.2020.115920

[46] M. Bhowmika, P. Kumari, G. Sarkar, M. Kanti Bainb, B. Bhowmick, M.M.R. Mollick, D. Mondal, D. Maity, D. Rana, D. Bhattacharjee, D. Chattopadhyay, Carbohydr. Polym. 62 (2013)

117-123;
https://doi.org/10.1016/j.ijbiomac.2013.08.024

[47] M.A. Al-Ghouti, Dana A. Da'ana, J. Hazard. Mater. 393 (2020) 122383;
https://doi.org/10.1016/j.jhazmat.2020.122383

[48] H.-K. Chung, W.-H. Kim, J. Park, J. Cho, T.-Y. Jeong, P.-K. Park, J. Ind. Eng. Chem. 28 (2015) 241-246; https://doi.org/10.1016/j.jiec.2015.02.021

[49] B. Q. Fu, J. H. Zuo, H. F. Zhao et al., Digest Journal of Nanomaterials and Biostructures, 2024, 19(4).